Experimental and theoretical lifetimes and transition probabilities in Sb I

Henrik Hartman[*] and Hampus Nilsson[†]
Department of Astronomy and Theoretical Physics, Lund University, Box 43, SE-221 00 Lund, Sweden

Lars Engström[‡] and Hans Lundberg[§]
Department of Physics, Lund University, Box 118, SE-221 00 Lund, Sweden

Patrick Palmeri,[‖] Pascal Quinet,[¶,††] and Émile Biémont[**,††]
Astrophysique et Spectroscopie, Université de Mons-UMONS, Place du Parc, 20, B-7000 Mons, Belgium
(Received 25 May 2010; published 15 November 2010)

We present experimental atomic lifetimes for 12 levels in Sb I. The levels belong to the $5p^2(^3P)6s\ ^2P$, ^4P, and $5p^2(^3P)5d\ ^4P$, ^4F, and ^2F terms. The lifetimes were measured using time-resolved laser-induced fluorescence. In addition, we report calculations of transition probabilities in Sb I using a multiconfigurational Dirac-Hartree-Fock method. The physical model was tested through comparisons between theoretical and experimental lifetimes for $5d$ and $6s$ levels. The lifetimes of the $5d\ ^4F_{3/2,5/2,7/2}$ levels (19.5, 7.8, and 54 ns, respectively) depend strongly on the J value. This is explained by different degrees of level mixing for the different levels in the ^4F term.

DOI: 10.1103/PhysRevA.82.052512 PACS number(s): 31.10.+z, 32.70.Cs

I. INTRODUCTION

As many other spectra, Sb I was first investigated by Meggers and Humphreys [1]. Since then the analysis has been extended and revised by Mazzoni and Joshi [2], Joshi *et al.* [3], Zaidi *et al.* [4], Beigang and Wynne [5], and Voss *et al.* [6]. The most recent and complete work is that of Hassini *et al.* [7], who reported 138 levels derived from 617 spectral lines measured in the range 2536 to 24 786 cm^{-1}, using Fourier transform spectroscopy. Of the reported levels 32 were previously unknown and several previous level assignments were revised. Furthermore, Hassini *et al.* [7] reported hyperfine splitting constants for more than 75% of the levels.

Belin *et al.* [8] measured radiative lifetimes of the two levels $(^3P)6s\ ^4P_{3/2}$ and $^4P_{5/2}$ using the Hanle-effect method. Andersen *et al.* [9] measured six levels [$(^3P)6s\ ^4P_{1/2,3/2,5/2}$, $^2P_{3/2}$, and $(^1D)6s\ ^2D_{3/2,5/2}$] using the beam-foil method. Furthermore, 14 lifetimes measured with beam foil, level crossing, and multichannel delayed-coincidence detection were reported by Osherovich and Tezikov [10] and Tezikov [11] for levels in the $6s$, $7s$, and $8s$ configurations.

Transition probabilities and lifetimes in neutral antimony are still very scarce. In astrophysics, this explains, e.g., why the most recent compilation of solar abundances [12] does not provide any result for the photospheric abundance of this element while the meteoritic result is well established. This is partly due to the fact that the lines identified as Sb I in the solar spectrum [13] are severely blended but also to the fact that reliable oscillator strengths are still lacking for these transitions.

In the present article, we report experimental lifetimes for 12 Sb I levels measured with time-resolved laser-induced fluorescence (TR-LIF) spectroscopy. In addition, we report calculated lifetimes and transition probabilities using a multiconfigurational Dirac-Hartree-Fock (MCDHF) method. The accuracy of the calculations is assessed through the good agreement observed between theoretical and available experimental lifetimes and branching fractions.

II. THE SB I TERM SYSTEM

The spectrum of neutral antimony (Sb I) is homologous with that of N I, with the lowest configuration ns^2np^3 (in Sb I, $n = 5$). Due to the Pauli exclusion principle, this configuration contains only three terms: $^4S^o$, $^2D^o$, and $^2P^o$, of which $^4S^o$ is the ground state. The system, with one excited p electron, can be written as $5s^25p^2\ nl$ and has the three parent terms, $^3P^o$, $^1D^o$, and $^1S^o$, which are the lowest terms in Sb II. The lowest even configuration is $(^3P)6s$ containing a ^4P and a ^2P term. There are no experimentally known levels belonging to the doubly excited system $5s^25p\ nln'l'$ or to the system where one or both of the $5s$ electrons are excited.

Figure 1 shows a partial energy level diagram of Sb I, including the levels measured in this work. Both terms in the $(^3P)6s$ configuration are plotted in Fig. 1, but only three of the six terms (^4P, ^4D, ^4F, ^2P, ^2D, and ^2F) in the $(^3P)5d$ configuration.

III. LIFETIME MEASUREMENTS

The lifetimes were measured at the Lund High Power Laser Facility (Sweden) using the TR-LIF technique. For a detailed description of the instrumentation, see Refs. [14–16].

A laser-produced plasma was created by focusing a 10-Hz frequency doubled Nd:YAG (yttrium aluminum garnet) laser onto a rotating antimony target, placed inside a vacuum chamber with a pressure of $\sim 10^{-5}$ mbar. The produced plasma

[*]Henrik.Hartman@astro.lu.se
[†]Hampus.Nilsson@astro.lu.se
[‡]Lars.Engstrom@fysik.lth.se
[§]Hans.Lundberg@fysik.lth.se
[‖]patrick.palmeri@umons.ac.be
[¶]Pascal.Quinet@ulg.ac.be
[**]E.Biemont@ulg.ac.be
[††]Also at IPNAS, Université de Liège, B-4000 Liège, Belgium.

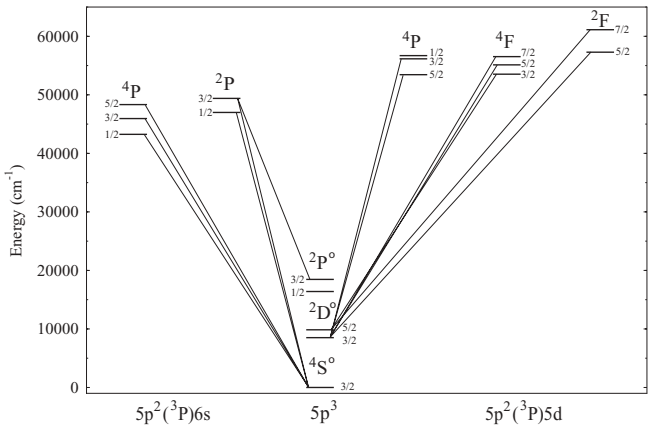

FIG. 1. Partial energy level diagram of Sb I, including the levels measured in this work. The lines connecting the levels show the excitation routes used for the LIF experiment.

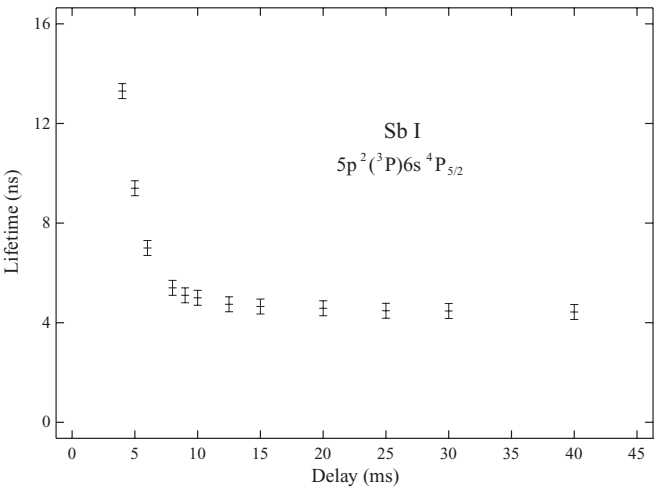

FIG. 2. Extracted lifetime of the $6s\ ^4P_{5/2}$ level as a function of the delay between the ablation and the excitation laser pulses, illustrating the severe saturation effect that occurs because the level is pumped from the ground state.

contained free antimony atoms in the ground and excited states. Antimony atoms in low-lying levels were selectively excited to the states under investigation and the subsequent fluorescence light was monitored as a function of time.

The atoms were excited by crossing the ablation plasma 1 cm above the target with a (typically) 1.2 ns duration pulse from a dye laser pumped by a Nd:YAG laser. The pump laser pulses were shortened using stimulated Brillouin scattering. The desired wavelengths were obtained using a 4-dicyanomethylene-2-methyl-6-*p*-dimethylaminostyryl-4H-pyran dye, making the laser tunable between 600 and 660 nm. β barium borate (BBO) and potassium diphosphate (KDP) doubling and tripling crystals were used to reach shorter wavelength. In addition, a hydrogen Raman shifter was used to change the frequency of the light by one or more Stokes or anti-Stokes shifts. The delay between the ablation and excitation pulses was tuned to make the plasma contain only slow atoms, decreasing flight-in and flight-out effects and collisional quenching. For all 6*s* levels, except $^2P_{3/2}$, the pumping laser was tuned to excite from the ground $^4S^o_{3/2}$ state (Fig. 1). Because of the strong reabsorption from the ground state, saturation effects turned out to be very important resulting in far too long experimental 6*s* lifetimes unless there was a long delay between the ablation and excitation laser pulses, leading to a plasma of sufficiently low density. This effect is clearly illustrated in Fig. 2. In the case of the $6s\ ^2P_{3/2}$ level, the excitation was from the $5p^3\ ^2P^o_{3/2}$ level where no such effect could be seen and a typical delay of around 5 μs was used.

The fluorescence signal was focused on a 1/8 m monochromator, equipped with a photomultiplier tube microchannel plate (Hamamatsu R1564) to detect the fluorescence signal. The laser pulse was detected separately with a photodiode. The fluorescence signal and the temporal shape of the laser pulse were recorded simultaneously with a transient digitizer and averaged over 1000 laser pulses. Typical curves are shown in Fig. 3.

The short lifetimes were extracted by least square fitting of the fluorescence signal with a single exponential convoluted with the shape of the laser pulse and a background function. Long lifetimes ($\tau > 10$ ns) were extracted by fitting a single exponential and a background function to the fluorescence signal after the excitation pulse had died off completely. When possible we used different channels for excitation and detection of the fluorescence and more than one pump and/or detection channel as seen in Table I. However, in some cases only one channel was accessible, and the pumping and detection had to be done in the same channel.

In Table I we report the excitation and detection (fluorescence) wavelengths, and the scheme used to excite the levels. The reported lifetimes in Table II are averages of 10 to 20 lifetime curves and the uncertainties quoted include both statistical and systematic uncertainties. For comparison we give values from previous experiments found in the literature. The fourth column gives our theoretical lifetimes calculated

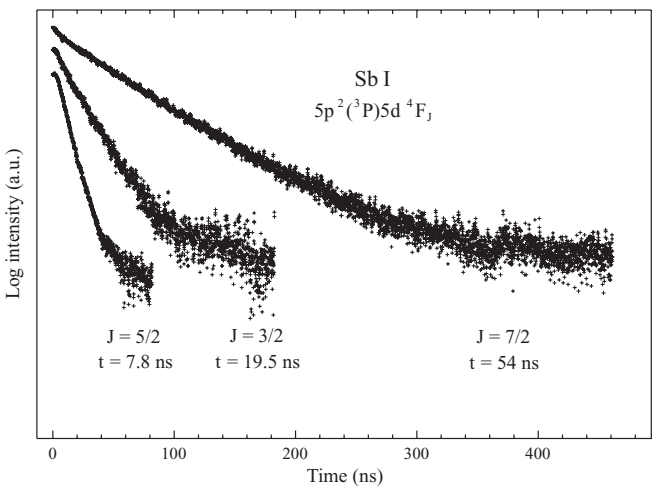

FIG. 3. Semilogarithmic plot of the decay of the different fine structure levels in the $5d\ ^4F$ term, illustrating the strong *J* dependence found in the lifetimes. The signal registered before and during the excitation laser pulse is omitted, and the data are not background corrected. The decay of the metastable $^4F_{9/2}$ level could not be measured.

TABLE I. Pumping scheme for Sb I levels. The first three columns are the pumped level under investigation, column 4 the lower level, column 5 the pumping transition, column 6 the fluorescence channel, and column 7 the level to which the fluorescence decays. The last column describes the technique used to produce desired frequency of the pumping radiation.

Config.[a]	Level[a]	E^a (cm^{-1})	Pump level	Pump λ (Å)	Fluorescence λ (Å)	Lower level	Method[b]
$5p^2(^3P)6s$	$^4P_{1/2}$	43 249.337	$^4S^o_{3/2}$	2311.463	2878	$^2D^o_{3/2}$	$3\omega + S$
$5p^2(^3P)6s$	$^4P_{3/2}$	45 945.340	$^4S^o_{3/2}$	2175.818	2176	$^4S^o_{3/2}$	3ω
$5p^2(^3P)6s$	$^4P_{5/2}$	48 332.424	$^4S^o_{3/2}$	2068.344	2068	$^4S^o_{3/2}$	3ω
$5p^2(^3P)6s$	$^2P_{1/2}$	46 991.058	$^4S^o_{3/2}$	2127.39	2599	$^2D^o_{3/2}$	3ω
$5p^2(^3P)6s$	$^2P_{3/2}$	49 391.133	$^4S^o_{3/2}$	2024.00	2529/3232	$^2D^o_{5/2}/^2P^o_{3/2}$	$3\omega + 2S$
			$^2P_{3/2}$	3232.53	2529/3232	$^2D^o_{5/2}/^2P^o_{3/2}$	2ω
$5p^2(^3P)5d$	$^4P_{5/2}$	53 442.967	$^2D^o_{3/2}$	2225.00	2290	$^2D^o_{5/2}$	3ω
$5p^2(^3P)5d$	$^4P_{3/2}$	56 151.802	$^2D^o_{3/2}$	2098.00	2098	$^2D^o_{3/2}$	3ω
$5p^2(^3P)5d$	$^4F_{3/2}$	53 527.956	$^2D^o_{3/2}$	2220.75	2850/2690/2280	$^2P^o_{1/2}/^2P^o_{3/2}/^2D^o_{3/2}$	3ω
$5p^2(^3P)5d$	$^4F_{5/2}$	55 120.943	$^2D^o_{3/2}$	2144.86	2208	$^2D^o_{5/2}$	3ω
$5p^2(^3P)5d$	$^4F_{7/2}$	56 528.132	$^2D^o_{5/2}$	2141.83	2142	$^2D^o_{5/2}$	3ω
$5p^2(^3P)5d$	$^2F_{5/2}$	57 287.052	$^2D^o_{3/2}$	2049.57	2050	$^2D^o_{3/2}$	3ω
$5p^2(^3P)5d$	$^2F_{7/2}$	61 125.741	$^2D^o_{5/2}$	1950.39	1950	$^2D^o_{5/2}$	3ω + AS

[a]From Hassini *et al.* [7].

[b]2ω and 3ω mean the second and the third harmonic; S and AS are written for the Stokes and anti-Stokes components of the Raman scattering.

with the MCDHF model and corrected by the experimental transition energies of Hassini *et al.* [7].

IV. CALCULATIONS IN SB I

In order to calculate the lifetimes of the $6s$ and $5d$ levels measured in this work, we have used the MCDHF method implemented in the GRASP2K computer package [17]. In this method, the atomic state functions (ASFs), $\Psi(\gamma J M_J)$, are expanded in linear combinations of configuration state functions (CSFs), $\Phi(\alpha_i J M_J)$, according to

$$\Psi(\gamma J M_J) = \sum_i c_i \Phi(\alpha_i J M_J). \tag{1}$$

The CSFs are in turn linear combinations of Slater determinants constructed from monoelectronic spin orbitals of the form

$$\varphi_{n\kappa m}(r,\theta,\phi) = \frac{1}{r}\begin{pmatrix} P_{n\kappa}(r)\chi_{\kappa m}(\theta,\phi) \\ i\,Q_{n\kappa}(r)\chi_{-\kappa m}(\theta,\phi) \end{pmatrix}, \tag{2}$$

where $P_{n\kappa}(r)$ and $Q_{n\kappa}(r)$ are, respectively, the large and the small component of the radial wave functions, and the angular functions $\chi_{\kappa m}(\theta,\phi)$ are the spinor spherical harmonics [18]. The α_i represent all the one-electron and intermediate quantum numbers needed to completely define the CSF. γ is usually chosen as the α_i corresponding to the CSF with the largest weight $|c_i|^2$. The quantum number κ is given by

$$\kappa = \pm\left(j + \tfrac{1}{2}\right), \tag{3}$$

where j is the electron total angular momentum. The sign before the parenthesis in Eq. (3) corresponds to the coupling relation between the electron orbital momentum, ℓ, and its spin, i.e.,

$$\ell = j \pm \tfrac{1}{2}. \tag{4}$$

The radial functions $P_{n\kappa}(r)$ and $Q_{n\kappa}(r)$ are numerically represented on a logarithmic grid and are required to be orthonormal within each κ symmetry. In the MCDHF variational procedure, the radial functions and the expansion coefficients c_i are optimized to self-consistency.

We considered the active space (AS) method for building the MCDHF multiconfiguration expansions. The latter are produced by exciting the electrons from the reference configurations to a given set of orbitals. The rules adopted for generating the configuration space differ according to the correlation model being used. Within a given correlation model, the AS of orbitals spanning the configuration space is increased to monitor the convergence of the total energies and the transition probabilities.

The MCDHF calculations were carried out in six steps. In the first step, the core orbitals, i.e., $1s$ to $4d$, together with the $5s$ and $5p$ orbitals, have been optimized. The six CSFs belonging to the ground configuration $5s^25p^3$ were retained in the configuration space. The energy functional was built within the framework of the average level (AL) option [18].

The second step consisted in increasing the configuration space by considering all the 62 CSFs belonging to the following configurations: $5s^25p^3 + 5s^25p^2\{6s,6p,5d\}^1$. The $6s, 6p$, and $5d$ orbitals have been optimized, keeping the others fixed to their values of the first step. The AL option was chosen to build the energy functional.

In the third step, the configuration space has been extended to 13 640 CSFs by considering the single and double virtual electron excitations to the active orbital set $\{5s,5p,5d,6s,6p,6d\}$ from the multireference configurations $5s^25p^3 + 5s^25p^2\{6s,6p,5d\}^1$. Only the $6d$ orbital has been optimized, fixing all the others to the values of the preceding step using an energy functional built from the lowest 62 ASFs within the framework of the extended optimal level (EOL) option [18]. One can note that, from this step of the computation

TABLE II. Comparison between experimental and calculated radiative lifetimes (τ in ns) in Sb I. Values marked with an asterisk were affected by convergence problems (see the text).

					Other studies	
Level[a]	E_{expt} (cm^{-1})[a]	E_{MCDHF} (cm^{-1})[b]	τ_{MCDHF} (ns)[b]	τ_{LIF} (ns)[c]	τ_{expt} (ns)	τ_{calc} (ns)
$(^3P)6s\ ^4P_{1/2}$	43 249.337	429 17	5.2(5.4)	5.3 ± 0.2	5.0 ± 0.4[d]	5.4[g]
					4.3 ± 0.4[f]	5.4(8.3)[h]
						4.1(7.5)[i]
$(^3P)6s\ ^4P_{3/2}$	45 945.340	454 19	5.6(5.4)	5.3 ± 0.2	4.9 ± 0.5[d]	5.1[g]
					5.1 ± 0.6[e]	5.3(7.8)[h]
					4.6 ± 0.5[f]	4.5(8.7)[i]
$(^3P)6s\ ^4P_{5/2}$	48 332.424	477 97	4.6(4.9)	4.6 ± 0.3	4.8 ± 0.4[d]	4.3[g]
					4.8 ± 0.6[e]	5.0(6.9)[h]
						4.5(8.9)[i]
$(^3P)6s\ ^2P_{1/2}$	46 991.058	467 83	3.2(3.2)	3.7 ± 0.2	5.2 ± 0.5[f]	3.7[g]
					5.5 ± 0.7[f]	2.7(3.7)[i]
$(^3P)6s\ ^2P_{3/2}$	49 391.133	492 17	3.9(3.6)	3.8 ± 0.2	4.0 ± 0.3[d]	3.9[g]
					4.3 ± 0.4[f]	4.0(5.0)[h]
						2.6(3.6)[i]
$(^1D)6s\ ^2D_{3/2}$	55 232.963	550 71	8.2(6.1)		3.7 ± 0.4[d]	4.4[g]
						4.3(6.3)[h]
						3.0(5.0)[i]
$(^1D)6s\ ^2D_{5/2}$	55 728.268	554 35	5.5(5.9)		3.8 ± 0.3[d]	4.7[g]
					3.9 ± 0.3[j]	5.2(7.1)[h]
						3.2(5.7)[i]
$(^3P)5d\ ^4P_{5/2}$	53 442.967	530 59	6.1(8.9)	7.0 ± 1.0		3.8[g]
$(^3P)5d\ ^4P_{3/2}$	56 151.802	556 83	5.3(5.5)	6.0 ± 0.4	4.1 ± 0.2[j]	3.7[g]
$(^3P)5d\ ^4P_{1/2}$	56 698.608	561 96	4.9(10.4)*		10.3 ± 0.7[f]	5.5[g]
$(^3P)5d\ ^4F_{3/2}$	53 527.956	534 38	23.4(23.2)	19.5 ± 1.5		11.3[g]
$(^3P)5d\ ^4F_{5/2}$	55 120.943	549 28	9.6(10.6)	7.8 ± 0.4		12.6[g]
$(^3P)5d\ ^4F_{7/2}$	56 528.132	562 65	60.8(59.8)	54 ± 3		30.4[g]
$(^3P)5d\ ^2P_{3/2}$	56 733.162	565 42	8.5(9.8)		3.5 ± 0.4[j]	3.6[g]
$(^3P)5d\ ^2F_{5/2}$	57 287.052	572 35	9.9(9.0)	9.5 ± 0.5		4.4[g]
$(^3P)5d\ ^2F_{7/2}$	61 125.734	609 41	3.8(4.1)	3.8 ± 0.3		2.7[g]
$(^3P)5d\ ^4D_{1/2}$	57 597.203	574 03	6.5(27.7)*		11.7 ± 0.8[f]	9.4[g]
$(^3P)5d\ ^4D_{5/2}$	58 862.889	586 84	6.3(13.7)*		10.4 ± 0.4[f]	10.6[g]

[a]Hassini *et al.* [7].
[b]MCDHF calculation (this work). The lifetimes are corrected from the experimental transition energies. a(b) stands for Babushkin(Coulomb).
[c]TR-LIF measurements (this work).
[d]Beam-foil spectroscopy [9].
[e]Hanle method [8].
[f]Delayed coincidence technique [10].
[g]HF + MC calculation [21]. We calculated the values for the 5*d* levels using the Hartree-Fock model kindly provided by the authors.
[h]MC + CI calculation [19]. a(b) stands for Babushkin(Coulomb).
[i]Relativistic OHFS calculation [20]. a(b) stands for length(velocity).
[j]Delayed coincidence technique [11].

and onward, core-valence and core-core correlations are also considered through the single and double excitations of the 5*s* core electrons, respectively.

The last three steps consisted in extending further the configuration space by adding to the active set of the preceding steps the following orbitals: 7*s*, 7*p*, and 7*d* in the fourth step giving rise to 41 603 CSFs; 8*s*, 8*p*, and 8*d* in the fifth step generating 85 130 CSFs; and finally, 4*f* in the last step with 118 912 CSFs generated. In these steps, only the added orbitals have been optimized, the others being fixed using the same energy functional as in the third step; also, single and double virtual electron excitations from the same multireference configurations as in the third step have been used to generate the configuration spaces. Further orbital additions to the active set as well as further opening of the core to include more core-valence and core-core correlations have been prevented by the memory limitations of our computer.

Two examples of convergence monitoring are shown in Fig. 4. The MCDHF lifetimes of the $(^3P)5d^2F_{7/2}$ and $(^3P)5d^4D_{1/2}$ levels as computed in the Babushkin and the Coulomb gauges are plotted as functions of the computation step. The values of the last step can be compared to our TR-LIF measurement for the $(^3P)5d^2F_{7/2}$ level and to the delayed coincidence measurement of Osherovich and Tezikov [10] for the $(^3P)5d^4D_{1/2}$ level. As one can see, in the case of

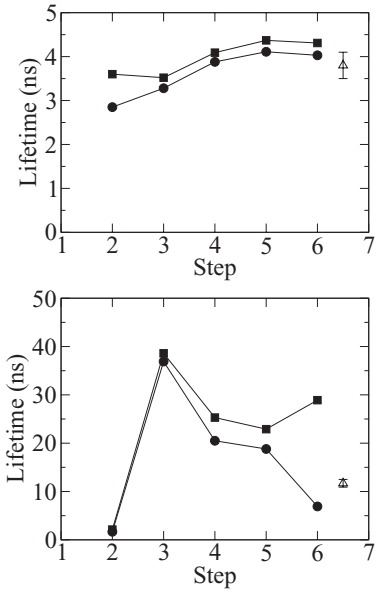

FIG. 4. Examples of convergence monitoring in which the MCDHF lifetime (in nanoseconds) is plotted as function of the computation step (see the text). Filled circles and the filled squares represent the Babushkin and the Coulomb gauge values, respectively. (Upper panel) $(^3P)5d^2F_{7/2}$ level; our TR-LIF measurement is shown with its error bar as an open triangle. (Lower panel) $(^3P)5d\ ^4D_{1/2}$ level; the measurement of Osherovich and Tezikov [10] is shown with its error bar as an open triangle.

$(^3P)5d^2F_{7/2}$, the calculated lifetime converges in both gauges to the experimental value, whereas it clearly diverges in the case of $(^3P)5d^4D_{1/2}$. The divergence of the MCDHF lifetime was also noticed for the $(^3P)5d^4D_{5/2}$,$^4P_{1/2}$ levels not shown here. These three $5d$ states are probably not properly represented due to missing correlations, e.g., with nf and ng ($n \geqslant 5$) orbitals.

In Table II, we report the MCDHF energies of the levels for which lifetime measurements are available. The corresponding MCDHF lifetimes and transition probabilities of main decay branches (presented in Table III) have been corrected by the experimental transition energies of Hassini *et al.* [7] as already stated in the previous section. Values affected by convergence problems are marked with an asterisk.

All the computed values reported here are without Breit and QED interactions. Rough estimates of the importance of these interactions on the lifetimes have been established in the second step of the computation; the lifetimes changed by less than 5%.

V. DISCUSSION

The 12 measured levels in Sb I are reported in Table II.

Comparing the TR-LIF lifetimes from this work with values in the literature, we agree within the uncertainties with Belin *et al.* [8] and Andersen *et al.* [9]. However, there is a clear discrepancy when comparing to Osherovich and Tezikov [10].

It is interesting to note that the lifetimes within the $5d\ ^4F$ term differ by more than a factor of 6; see Fig. 3. Only the three levels with the lowest J values (3/2, 5/2, and 7/2) are measured in this term. The level with the highest J value, $^4F_{9/2}$, is metastable since there are no odd levels with $J \geqslant 7/2$ below 57 000 cm^{-1} to which it can decay through an electric dipole transition. The shortest lifetime is that of $J = 5/2$ (7.8 ns). This can be explained by the large mixing with $5d\ ^4P_{5/2}$ which opens up a strong decay channel to the ground level $^4S^o_{3/2}$, decreasing the lifetime. The level $5d\ ^4F_{3/2}$ mixes with $5d\ ^4P_{3/2}$, but not as much as in the previous case, and the transition to $^4S^o_{3/2}$ is weaker, giving the longer lifetime of 19.5 ns. The level $5d\ ^4F_{7/2}$ has a too large J value to mix with the $5d\ ^4P$ since level mixing can only occur between levels with the same J value. However, this level is mixed with ^2F, opening up the channel down to $5p^3\ ^2D^o_{5/2}$. The experimental lifetimes for the levels in the ^4F term are nicely reproduced by the theoretical calculation. The MCDHF level energies are compared with the experimental data of Hassini *et al.* [7] in Table II (see column 3). The agreement is excellent.

A comparison between experimental and calculated lifetimes is also shown in Table II. The calculated level energies appear systematically but consistently lower than the experimental results by a few hundred cm^{-1}. Our MCDHF calculations are in agreement with our LIF measurements and with the values of Belin *et al.* [8] and Andersen *et al.* [9], whereas the values of Osherovich and Tezikov [10] seem to have larger uncertainties than quoted.

A good agreement is found between our MCDHF and TR-LIF lifetimes with most of the calculated values being within the error bars. Moreover, one can observe the good agreement between the Coulomb and Babushkin gauges for most of the MCDHF lifetimes. This is a necessary but not a sufficient condition for the accuracy of the calculations. It should be emphasized that this agreement was not observed in the earlier MC + configuration interaction (CI) [19] and optimized Hartree Fock Slater (OHFS) calculations [20]. Discrepancies between the two gauges reaching a factor of 2 and more are, however, observed for the three high excitation levels at 56 698, 57 597, and 58 862 cm^{-1} due to the convergence problems mentioned in the previous section. Albeit the HF + MC calculations of Gonzalez *et al.* [21] show an excellent agreement with our measurements for the $6s$ levels, we have a completely different situation as far as the $5d$ levels are concerned. The latter were not published in Ref. [21] and we have therefore calculated them using the model kindly provided by these authors.

Regarding the previous measurements, the beam-foil data [9] and the Hanle measurements [8] have been confirmed by our TR-LIF lifetimes, while the beam-foil values for the $6s\ ^2D_{3/2,5/2}$ levels are significantly shorter than our MCDHF predictions. The problem is probably originating from the MCDHF values because these two $6s\ ^2D$ levels are strongly mixed with $5d$ levels (which is not the case for the other levels of the same configuration), the dominant percentages being less than 25% in jj coupling for these two levels. The better agreement theory-experiment observed for the HF + MC is probably due to the fact that the authors of Ref. [21] used a semiempirical optimization procedure, the results of the present work being purely theoretical.

The delay coincidence measurements of Osherovich and Tezikov [10] and of Tezikov [11] are, on the other hand, found

TABLE III. Transition probabilities (A_{ki}), weighted oscillator strengths (gf_{ik}), and branching fractions (BF) of decay transitions depopulating the even levels reported in Table II. Only transitions with wavelengths $\lambda \leqslant 2500$ nm and $A_{ki} \geqslant 1.00 \times 10^6$ are quoted. r is the ratio between Babushkin and Coulomb gauges. Values marked with an asterisk were affected by convergence problems (see the text).

Upper level[a]	Lower level[a]	λ(nm)[a]	A_{ki} (s^{-1})[b]	r	gf_{ik}[b]	BF[b]
$6s\ ^4P_{1/2}$	$5p^3\ ^4S^o_{3/2}$	231.146	1.60×10^8	1.045	2.56×10^{-1}	8.25×10^{-1}
	$5p^3\ ^2D^o_{3/2}$	287.791	3.21×10^7	1.092	7.99×10^{-2}	1.66×10^{-1}
	$5p^3\ ^2P^o_{3/2}$	403.354	1.47×10^6	1.610	7.17×10^{-3}	7.59×10^{-3}
$6s\ ^4P_{3/2}$	$5p^3\ ^4S^o_{3/2}$	217.582	1.59×10^8	0.946	4.51×10^{-1}	8.89×10^{-1}
	$5p^3\ ^2D^o_{3/2}$	267.063	6.55×10^6	1.224	2.80×10^{-2}	3.67×10^{-2}
	$5p^3\ ^2D^o_{5/2}$	276.993	1.19×10^7	0.930	5.47×10^{-2}	6.66×10^{-2}
$6s\ ^2P_{1/2}$	$5p^3\ ^4S^o_{3/2}$	212.739	3.82×10^6	0.479	5.18×10^{-3}	1.21×10^{-2}
	$5p^3\ ^2D^o_{3/2}$	259.805	2.83×10^8	1.040	5.72×10^{-1}	8.97×10^{-1}
	$5p^3\ ^2P^o_{1/2}$	326.749	2.84×10^7	0.976	9.08×10^{-2}	9.00×10^{-2}
$6s\ ^4P_{5/2}$	$5p^3\ ^4S^o_{3/2}$	206.834	1.97×10^8	1.070	7.60×10^{-1}	9.04×10^{-1}
	$5p^3\ ^2D^o_{5/2}$	259.808	2.03×10^7	1.009	1.23×10^{-1}	9.29×10^{-2}
$6s\ ^2P_{3/2}$	$5p^3\ ^4S^o_{3/2}$	202.400	1.06×10^6	0.270	2.60×10^{-3}	4.13×10^{-3}
	$5p^3\ ^2D^o_{3/2}$	244.550	7.75×10^6	1.305	2.78×10^{-2}	3.03×10^{-2}
	$5p^3\ ^2D^o_{5/2}$	252.851	2.19×10^8	0.940	8.40×10^{-1}	8.55×10^{-1}
	$5p^3\ ^2P^o_{1/2}$	302.981	1.81×10^7	1.000	9.95×10^{-2}	7.05×10^{-2}
	$5p^3\ ^2P^o_{3/2}$	323.249	1.03×10^7	0.520	6.47×10^{-2}	4.03×10^{-2}
$5d\ ^4P_{5/2}$	$5p^3\ ^4S^o_{3/2}$	187.115	1.50×10^8	1.471	4.72×10^{-1}	9.16×10^{-1}
	$5p^3\ ^2D^o_{3/2}$	222.495	9.64×10^6	1.148	4.30×10^{-2}	5.90×10^{-2}
	$5p^3\ ^2D^o_{5/2}$	229.345	2.33×10^6	1.069	1.10×10^{-2}	1.42×10^{-2}
$5d\ ^4F_{3/2}$	$5p^3\ ^4S^o_{3/2}$	186.818	9.04×10^6	0.615	1.89×10^{-2}	2.11×10^{-1}
	$5p^3\ ^2D^o_{3/2}$	222.075	8.72×10^6	0.765	2.58×10^{-2}	2.04×10^{-1}
	$5p^3\ ^2D^o_{5/2}$	228.899	7.31×10^6	1.417	2.30×10^{-2}	1.71×10^{-1}
	$5p^3\ ^2P^o_{1/2}$	269.225	4.46×10^6	1.143	1.94×10^{-2}	1.04×10^{-1}
	$5p^3\ ^2P^o_{3/2}$	285.111	1.30×10^7	1.712	6.32×10^{-2}	3.03×10^{-1}
$5d\ ^4F_{5/2}$	$5p^3\ ^4S^o_{3/2}$	181.419	4.09×10^7	1.786	1.21×10^{-1}	3.92×10^{-1}
	$5p^3\ ^2D^o_{3/2}$	214.484	3.02×10^7	0.647	1.25×10^{-1}	2.90×10^{-1}
	$5p^3\ ^2P^o_{3/2}$	272.720	1.37×10^7	0.980	9.15×10^{-2}	1.31×10^{-1}
$6s\ ^2D_{3/2}$	$5p^3\ ^4S^o_{3/2}$	181.051	4.35×10^7	0.737	8.56×10^{-2}	3.57×10^{-1}
	$5p^3\ ^2D^o_{3/2}$	213.970	7.10×10^7	0.861	1.95×10^{-1}	5.82×10^{-1}
	$5p^3\ ^2P^o_{1/2}$	257.405	6.55×10^6	1.065	2.60×10^{-2}	5.36×10^{-2}
$6s\ ^2D_{5/2}$	$5p^3\ ^2D^o_{3/2}$	211.725	1.21×10^7	2.563	4.87×10^{-2}	6.68×10^{-2}
	$5p^3\ ^2D^o_{5/2}$	217.919	1.67×10^8	0.988	7.16×10^{-1}	9.27×10^{-1}
$5d\ ^4P_{3/2}$	$5p^3\ ^4S^o_{3/2}$	178.089	4.40×10^7	1.375	8.36×10^{-2}	2.34×10^{-1}
	$5p^3\ ^2D^o_{3/2}$	209.842	1.11×10^8	1.037	2.93×10^{-1}	5.90×10^{-1}
	$5p^3\ ^2D^o_{5/2}$	215.925	5.08×10^6	1.248	1.42×10^{-2}	2.70×10^{-2}
	$5p^3\ ^2P^o_{1/2}$	251.456	4.76×10^6	1.063	1.81×10^{-2}	2.53×10^{-2}
	$5p^3\ ^2P^o_{3/2}$	265.260	2.33×10^7	0.673	9.83×10^{-2}	1.24×10^{-1}
$5d\ ^4F_{7/2}$	$5p^3\ ^2D^o_{5/2}$	214.184	1.63×10^7	0.982	9.00×10^{-2}	9.94×10^{-1}
$5d\ ^4P_{1/2}$	$5p^3\ ^4S^o_{3/2}$	176.309	$6.17 \times 10^{6*}$	0.081^*	$5.75 \times 10^{-3*}$	$3.03 \times 10^{-2*}$
	$5p^3\ ^2P^o_{1/2}$	248.044	$5.24 \times 10^{6*}$	0.840^*	$9.68 \times 10^{-3*}$	$2.57 \times 10^{-2*}$
	$5p^3\ ^2P^o_{3/2}$	261.466	$1.85 \times 10^{8*}$	13.603^*	$3.79 \times 10^{-1*}$	$9.07 \times 10^{-1*}$
$5d\ ^2P_{3/2}$	$5p^3\ ^4S^o_{3/2}$	176.202	1.84×10^7	1.920	3.43×10^{-2}	1.57×10^{-1}
	$5p^3\ ^2D^o_{3/2}$	207.312	1.94×10^6	0.576	5.01×10^{-3}	1.65×10^{-2}
	$5p^3\ ^2P^o_{1/2}$	247.832	2.47×10^7	1.016	9.11×10^{-2}	2.10×10^{-1}
	$5p^3\ ^2P^o_{3/2}$	261.230	7.09×10^7	1.103	2.90×10^{-1}	6.04×10^{-1}
$5d\ ^2F_{5/2}$	$5p^3\ ^4S^o_{3/2}$	174.560	1.08×10^6	0.400	2.96×10^{-3}	1.07×10^{-2}
	$5p^3\ ^2D^o_{3/2}$	204.958	9.93×10^7	0.919	3.75×10^{-1}	9.81×10^{-1}

TABLE III. *(Continued.)*

Upper level[a]	Lower level[a]	λ(nm)[a]	A_{ki} (s^{-1})[b]	r	gf_{ik}[b]	BF[b]
$5d\ ^4D_{1/2}$	$5p^3\ ^4S^o_{3/2}$	173.557	$2.74 \times 10^{6*}$	0.197*	$2.48 \times 10^{-3*}$	$1.78 \times 10^{-2*}$
	$5p^3\ ^2P^o_{1/2}$	242.634	$2.05 \times 10^{7*}$	0.949*	$3.62 \times 10^{-2*}$	$1.33 \times 10^{-1*}$
	$5p^3\ ^2P^o_{3/2}$	255.462	$1.27 \times 10^{8*}$	2275.0*	$2.48 \times 10^{-1*}$	$8.21 \times 10^{-1*}$
$5d\ ^4D_{5/2}$	$5p^3\ ^4S^o_{3/2}$	169.823	$3.39 \times 10^{6*}$	0.521*	$8.81 \times 10^{-3*}$	$2.13 \times 10^{-2*}$
	$5p^3\ ^2D^o_{3/2}$	198.542	$5.57 \times 10^{7*}$	2.040*	$1.98 \times 10^{-1*}$	$3.50 \times 10^{-1*}$
	$5p^3\ ^2D^o_{5/2}$	203.979	$3.86 \times 10^{7*}$	1.191*	$1.45 \times 10^{-1*}$	$2.42 \times 10^{-1*}$
	$5p^3\ ^2P^o_{3/2}$	247.458	$6.09 \times 10^{7*}$	10.130*	$3.36 \times 10^{-1*}$	$3.82 \times 10^{-1*}$
$5d\ ^2F_{7/2}$	$5p^3\ ^2D^o_{5/2}$	195.039	2.60×10^{8}	1.070	1.18×10^{0}	9.97×10^{-1}

[a]Hassini *et al.* [7]. The wavelengths are determined from the experimental energy levels and are given in air when longer than 200 nm.
[b]MCDHF calculation (this work). The MCDHF values are corrected from the experimental transition energies. Only the Babushkin gauge results are quoted.

to be significantly shorter or longer than our experimental and theoretical lifetimes. This is also true for the $6s\ ^2P_{1/2}$ level where the only previous experimental lifetimes are obtained by the delayed coincidence technique [10,11]. However, we note that in their branching fraction measurements Guern and Lotrian [22] proposed a lifetime of 3.7 ± 0.7 ns for this level from a Boltzmann plot. This value is in close agreement with both our TR-LIF and MCDHF results.

The corrected MCDHF transition probabilities, along with the corresponding oscillator strengths and branching fractions, are reported in Table III for the main decay transitions depopulating the even levels presented in Table II. A good agreement between the gauges is generally found for the strong lines except for the lines depopulating the three high excitation levels $(^3P)5d\ ^4D_{1/2,5/2}$ and $(^3P)5d\ ^4P_{1/2}$ due to the convergence problems mentioned in the previous section.

In Fig. 5, our calculated branching fractions (in the Babushkin gauge) as reported in Table III are compared to the measurements of Guern and Lotrian [22] and of Gonzalez *et al.* [21]. The averages of the ratios BF_{expt}/BF_{MCDHF} for the strong branches ($BF_{MCDHF} \geqslant 0.1$) excluding the values for the decay transition $6s\ ^2D_{3/2}$–$5p^3\ ^4S^o_{3/2}$, for which there is a disagreement of up to a factor of 2, are respectively 0.99 ± 0.12 for Guern and Lotrian [22] and 0.97 ± 0.08 for Gonzalez *et al.* [21] (the quoted uncertainties being the standard deviation to the mean) showing a reasonable agreement between the three data sets. Concerning the BF of the transition $6s\ ^2D_{3/2}$–$5p^3\ ^4S^o_{3/2}$, the strong disagreement between theory and experiment is due to the inaccuracy of the MCDHF A value for the decay branch $6s\ ^2D_{3/2}$–$5p^3\ ^2P^o_{3/2}$ ($9.33 \times 10^5\ s^{-1}$ in the Babushkin gauge and $1.44 \times 10^7\ s^{-1}$ in the Coulomb gauge) that is involved in the calculation of the BF of the decay branch $6s\ ^2D_{3/2}$–$5p^3\ ^4S^o_{3/2}$.

Our corrected MCDHF transition probabilities (in the Babushkin gauge) are compared with the available theoretical data in the literature (Refs. [19–21]) in Fig. 6. The relativistic OHFS A-values of Holmgren [20] for the strong lines ($A \geqslant 10^8\ s^{-1}$) are definitely too high. The agreement is somewhat better with the other two theoretical methods [19,21] for the

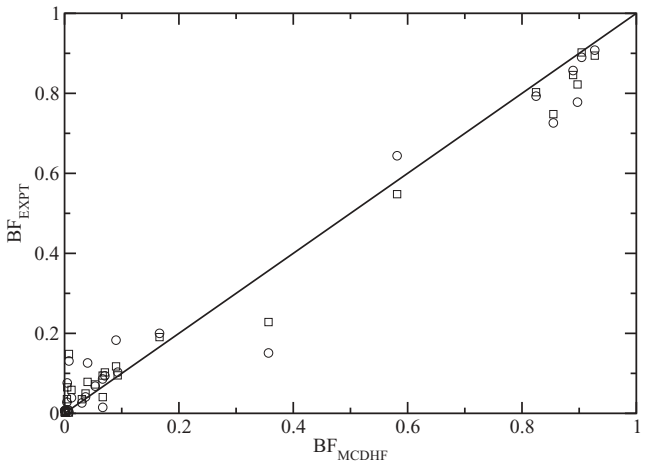

FIG. 5. Comparison between corrected MCDHF (in the Babushkin gauge) and experimental branching fractions (BFs). Circles: Guern and Lotrian [22]. Squares: Gonzalez *et al.* [21]. A straight line of equality is drawn.

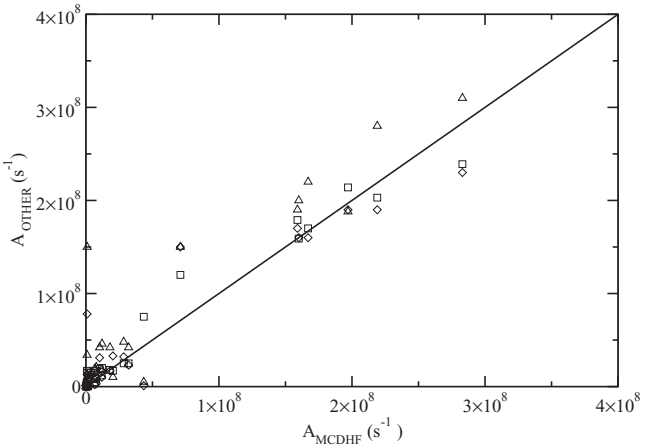

FIG. 6. Comparison between corrected MCDHF transition probabilities (in the Babushkin gauge) and theoretical values taken from the literature. Squares: HF + MC calculation [21]. Diamonds: MC + CI calculation (in the Babushkin gauge) [19]. Triangles: relativistic OHFS calculation (in the length gauge) [20]. A straight line of equality is drawn.

strong lines if we except the transition $6s\ ^2P_{1/2}$–$5p^3\ ^2D^o_{3/2}$ with $A_{\mathrm{MCDHF}} = 2.83 \times 10^8$ (Babushkin) and 2.72×10^8 (Coulomb) s^{-1}. The HF + MC [21] and MC + CI [19] results are predicted too low (length gauge) for that transition, i.e., 2.39×10^8 and 2.30×10^8 s^{-1}, respectively. Unfortunately, both authors did not publish their velocity-gauge A values. Nonetheless, all these three "old" calculations are expected to be less accurate than the present results due to the consideration of configuration interaction effects in a more limited way.

ACKNOWLEDGMENTS

This work was financially supported by the Integrated Initiative of Infrastructure Project LASERLAB-EUROPE, Contract No. RII3-CT-2003-506350, the Swedish Research Council through the Linnaeus grant, the Knut and Alice Wallenberg Foundation, and the Belgian FRS-FNRS. We thank our Spanish colleagues (A. M. Gonzalez, M. Ortiz, and J. Campos) for providing us with some details about their calculations.

[1] W. F. Meggers and C. J. Humphreys, J. Res. Natl. Bur. Std. **28**, 463 (1942).

[2] M. Mazzoni and Y. N. Joshi, Physica B + C **97**, 107 (1979).

[3] Y. N. Joshi, V. N. Sarma, and T. A. M. Van Kleef, Physica B + C **125**, 127 (1984).

[4] A. A. Zaidi, Y. Makdisi, and K. S. Bhatia, J. Phys. B **17**, 355 (1984).

[5] R. Beigang and J. J. Wynne, J. Opt. Soc. Am. B **3**, 949 (1986).

[6] M. Voss, W. Weise, H. Buchenholz, and R. Winkler, Z. Phys. D **1**, 151 (1986).

[7] F. Hassini, Z. B. Ahmed, O. Robaux, J. Vergès, and J.-F. Wyart, J. Opt. Soc. Am. B **5**, 2060 (1988).

[8] G. Belin, S. Garpman, L. Holmgren, and S. Rydberg, Phys. Scr. **9**, 213 (1974).

[9] T. Andersen, S. Worre Jorgensen, and G. Sorensen, J. Opt. Soc. Am. **64**, 891 (1974).

[10] V. V. Tezikov, Opt. Spectrosc. **44**, 121 (1978).

[11] A. L. Osherovich and V. V. Tezikov, Opt. Spectrosc. **43**, 612 (1977).

[12] N. Grevesse, M. Asplund, A. J. Sauval, and P. Scott, Astrophys. Space Sci. (to be published).

[13] C. E. Moore, M. G. J. Minnaert, and J. Houtgast, NBS Monograph 61, U.S. Department of Commerce, 1966.

[14] H. Bergström, H. Faris, G. W. Hallstadius, H. Lundberg, A. Persson, and C. G. Wahlström, Z. Phys. D **8**, 17 (1988).

[15] H. L. Xu, S. Svanberg, P. Quinet, H. P. Garnir, and É. Biémont, J. Phys. B **36**, 4773 (2003).

[16] H. L. Xu, A. Persson, S. Svanberg, K. Blagoev, G. Malcheva, V. Pentchev, É. Biémont, J. Campos, M. Ortiz, and R. Mayo, Phys. Rev. A **70**, 042508 (2004).

[17] P. Jonsson, X. He, C. Froese Fischer, and I. P. Grant, Comput. Phys. Commun. **177**, 597 (2007).

[18] I. P. Grant, in *Methods of Computational Chemistry*, edited by S. Wilson (Plenum Press, New York, 1988), Vol. 2, pp. 1–71.

[19] J. R. Bieron and J. Migdalek, J. Phys. B **25**, 4099 (1992).

[20] L. Holmgren, Phys. Scr. **11**, 15 (1975).

[21] A. M. Gonzalez, M. Ortiz, and J. Campos, J. Quant. Spectrosc. Radiat. Transfer **57**, 825 (1997).

[22] Y. Guern and J. Lotrian, J. Quant. Spectrosc. Radiat. Transfer **24**, 133 (1980).